Progress In Electromagnetics Research, Vol. 176, 35–44, 2023

Highly Transparent Tunable Microwave Perfect Absorption for Broadband Microwave Shielding

Dongdong Li[1, 2, 3], Xiaojun Hu[1, 2, 3], Bingtao Gao[1, 2, 3, *], Wen-Yan Yin[1, 2, 3, *], Hongsheng Chen[1, 2, 3, *], and Haoliang Qian[1, 2, 3, *]

Abstract—To shield undesirable microwave radiation to protect electronic systems and human health, microwave perfect absorbers have attracted increasing interests in recent years. However, the opaque or semitransparent nature of most implemented microwave absorbers limit their applications in optics. Here, we demonstrate a high-performance microwave absorber based on an impedance-assisted Fabry-Pérot resonant cavity with an ITO-dielectric-ITO structure without complex nanofabrication. The device features near-unity absorption (99.5% at 14.4 GHz with a 4.5 GHz effective bandwidth), excellent electromagnetic interference shielding performance (24 dB) in the Ku-band, and high optical transparency (89.0% from 400 nm to 800 nm). The peak absorption frequency of the device can be tuned by changing the thickness of glass slab and sheet resistance of ITO films. Our work provides a low-cost and feasible solution for high-performance optically transparent microwave shielding and stealth, paving the way towards applications in areas of microwave and optics.

1. INTRODUCTION

Electronic devices have brought great convenience to daily life, yet the development of modern electronics and microwave wireless communication is also accompanied with a type of serious microwave pollution. Strong microwave interference not only threatens human health, but also is harmful to electromagnetic equipment operation; therefore, microwave shielding technologies are important to high-precision devices, especially in the field of military, aerospace, and telecommunications [1–3]. Traditional metals and emerging shielding materials such as metal-organic framework architectures [4], basalt fabric/epoxy composites [5], or MXene composites [6–10] have good shielding effectiveness. Nevertheless, their opaqueness would limit applications in some fields of optoelectronics, for example, glass for stealth aircrafts or warships [11] or optical detection devices for medical and electronic security purposes [12, 13]. Considerable efforts have been devoted to developing optical transparent microwave shielding materials, such as nanoscale metal meshes [14–16], carbon-based composites [17], carbon nanotubes [18], and graphene [3], but to date effective transparent microwave shielding is still challenging.

As an effective device to achieve microwave shielding, microwave absorbers (MAs), utilizing the coupling between electromagnetic waves and materials to produce Joule heat, can effectively reduce microwave transmission and reflection [19, 20]. In the past decades, MAs represented by composites containing ferrite or magnetic metal particles have been widely studied due to remarkable microwave absorption [21–23], but they are usually opaque due to high optical reflection and/or absorption resulting

Received 19 October 2022, Accepted 17 November 2022, Scheduled 27 November 2022

* Corresponding authors: Bingtao Gao (bgao@zju.edu.cn), Wen-Yan Yin (wyyin@zju.edu.cn), Hongsheng Chen (hansomchen@zju.edu.cn), Haoliang Qian (haoliangqian@zju.edu.cn).

[1] Interdisciplinary Center for Quantum Information, State Key Laboratory of Modern Optical Instrumentation, ZJU-Hangzhou Global Scientific and Technological Innovation Center, Zhejiang University, Hangzhou 310027, China. [2] International Joint Innovation Center, Key Lab. of Advanced Micro/Nano Electronic Devices & Smart Systems of Zhejiang, The Electromagnetics Academy at Zhejiang University, Zhejiang University, Haining 314400, China. [3] Jinhua Institute of Zhejiang University, Zhejiang University, Jinhua 321099, China.

from high permeability and wide optical absorption band. To achieve high optical transparency and perfect microwave absorption, the transparent microwave absorption materials such as ITO, graphene, and PET are considered promising to enhance microwave absorption by designing resonant structure. Furthermore, the metamaterial MAs based on these materials have been proposed and shown to achieve semitransparent MAs by impedance matching to minimize reflection [24–27]. However, the undesired narrow bandwidth poor transparency high production costs and complex fabrication process will critically limit their practical applications.

In this work, we propose a universal approach to design visible high transparent perfect MAs based on a Fabry-Pérot cavity using a glass slab sandwiched in two ITO films with different sheet resistances to form an ITO-dielectric-ITO (IDI) resonant structure (Fig. 1(a)). Here, the ITO films with high and low sheet resistances function like an impedance matching layer and a microwave reflector, respectively. The glass slab acts as the dielectric spacer to provide a phase difference for destructive interference, and critical coupling in cavity can be realized by selecting the thickness of glass slab. We theoretically calculate and analyze the microwave properties by employing the multi-beam interference theory. Results show that the maximum achievable microwave absorption of the proposed device is near-unity (99.5%) with a 90% bandwidth about 4.5 GHz, and the minimum reflection is −50.0 dB. Furthermore, we theoretically prove that the ITO films contribute equivalently to the microwave absorption. For demonstration, we then implement the experiment to characterize the microwave and optical properties, which shows the maximum microwave absorption 97.7% at 14.3 GHz with a 3 GHz effective bandwidth for TE10 mode, which is in good agreement with our theoretical analysis, and the optical transmission reaches 89.0%.

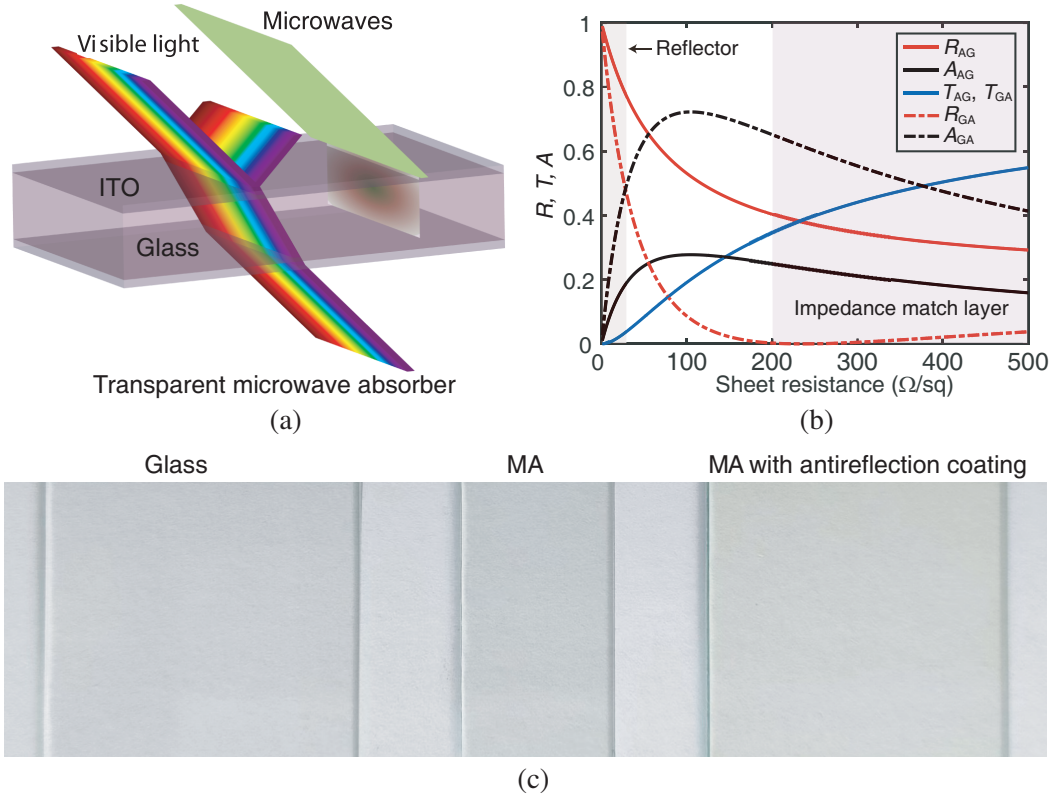

Figure 1. (a) Schematic of the proposed transparent MA. (b) Microwave performance at 15 GHz of single ITO film at the air-glass interface changing with the sheet resistance; R_{AG}, T_{AG}, and A_{AG} normal incidence from air to glass; R_{GA}, T_{GA}, and A_{GA} normal incidence from glass to air. (c) Optical image of glass and MAs without and with an antireflection coating when the sheet resistance of bottom ITO film is 10 Ω/sq, and that of top ITO film is 500 Ω/sq.

2. RESULTS AND DISCUSSION

2.1. Design and Fabrication of the Transparent Microwave Absorber

The microwave absorption by a single ITO film is usually limited by high reflection for low sheet resistance arising from impedance mismatch, or by high transmission for high sheet resistance due to nanoscale thickness. However, the tunable microwave characteristics and high optical transparency make it excellent candidates to design transparent MAs. Fig. 1(a) shows the schematic of the proposed transparent MA. Microwave reflection (R), transmission (T), and absorption (A) of a single ITO film on top of a semi-infinite glass slab are related to its sheet resistance (SR) and the direction of the incident wave. Fig. 1(b) shows the theoretical results of incidence from air to glass (R_{AG}, T_{AG}, A_{AG}) and from glass to air (R_{GA}, T_{GA}, A_{GA}). The derivations of R, T, and A are discussed in Supporting Information (see supply materials S1 for more details). Note that T_{AG} is the same as T_{GA} since the structure is reciprocal. In the range up to $500\,\Omega/\mathrm{sq}$, films with lower sheet resistance have higher microwave reflection, hence can be used as a microwave reflector on the back. In contrast, those with higher sheet resistance have lower microwave reflection but higher microwave transmission, and can be selected as the top layer to improve impedance match when designing MAs. Both the ITO films provide microwave absorption. Combining the advantages of different ITO films, through reasonable designs, we can achieve high-performance MAs with low reflection and transmission.

In this work, we study the effects of glass thickness, sheet resistance of ITO films, and incidence angle on the performance of proposed transparent MA, showing tunable perfect MAs for broadband microwave shielding. For increasing the optical transmittance of MAs, the antireflection coating is employed. The optical images of the glass and proposed MAs shown in Fig. 1(c) indicate high transparency and good visual experience of the device. In addition, the proposed IDI-structured resonant cavity has very low cost and can be easily fabricated without a complex structure and nanofabrication, demonstrating their great commercial and industrial potential for high-performance microwave shielding applications.

2.2. Principles of Perfect Microwave Absorption and Effects of Cavity Properties

For understanding the proposed transparent MA, we adopt an analytical method to theoretically study the condition for perfect microwave absorption by employing the multi-beam interference theory. Without losing generality, we consider that an MA is placed with medium 1 above and medium 3 below, as shown in Fig. 2(a). The ITO films are considered as a 2D boundary condition due to its ultrathin thickness compared with microwave wavelength, which is characterized by their sheet resistance SR_{ij} $(i, j = 1, 2, 3)$ in the interface of medium i and medium j. The structure can be modeled as an impedance-assisted Fabry-Pérot resonant cavity consisting of two impedance boundaries. Here, we ignore any near-field coupling between the impedance surfaces and only consider the reflection coupling occurring between the two surfaces for this cavity. The total reflection and transmission of such a structure can be regarded as the superposition of transmitted and reflected microwave on the interfaces, which can be expressed explicitly as [28]

$$r_{\mathrm{total}} = r_{12} + t_{12}r_{23}t_{21} \cdot \frac{e^{i\cdot 2k_z d}}{1 - r_{21}r_{23} \cdot e^{i\cdot 2k_z d}},$$
$$t_{\mathrm{total}} = t_{12}t_{23} \cdot \frac{e^{i\cdot 2k_z d}}{1 - r_{21}r_{23} \cdot e^{i\cdot 2k_z d}},$$

where r_{ij} and t_{ij} are the reflection and transmission coefficients when traveling from medium i to j (see Section S1 of the Supporting Information for details); d denotes the thickness of the medium 2; and k_z is the propagation constant in z direction inside the medium 2. Note that any highly transparent material can be used for medium 2. Here, the glass-slab is used due to its high optical transmittance, low price, and wide application scenarios.

For a Fabry-Pérot cavity, resonance can be treated as a phase-matching problem, and to achieve the resonant absorption, the self-consistency condition must be satisfied, which leads to $2k_z d + \theta_{23} + \theta_{21} = 2m\pi$, where θ_{ij} is the phase corresponding to the reflection coefficient r_{ij}, and m is the order of resonance. The absorption spectrum curve can be calculated according to $A(\omega) = 1 - T(\omega) - R(\omega)$. Fig. 2(b) shows

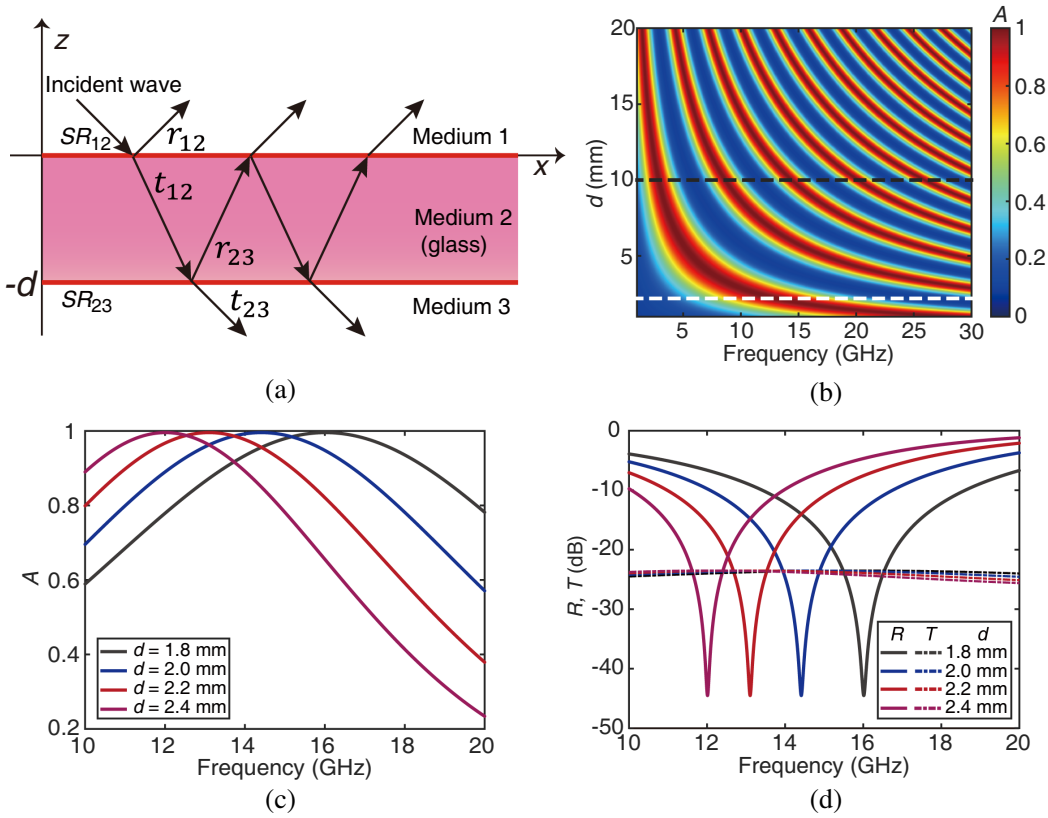

Figure 2. (a) Schematic depicting the partial reflection and transmission coefficients at the transparent MA interfaces. (b) Calculated microwave absorption spectra as a function of glass-slab thickness d. (c), (d) Effects of d on (c) A and (d) R and T of MA for normal incidence. Here, $SR_{12} = 450\,\Omega/\text{sq}$ and $SR_{23} = 10\,\Omega/\text{sq}$.

the calculated microwave absorption changing with the glass-slab thickness d (from 1 mm to 20 mm) at different microwave excitation frequencies for $SR_{12} = 450\,\Omega/\text{sq}$ and $SR_{23} = 10\,\Omega/\text{sq}$. The microwave absorption peak appears periodically with the increase or decrease of d at a particular excitation frequency or the frequencies when glass-slab thickness is fixed (such as $d = 10$ mm) shown in Fig. 2(b). Specifically, when the glass-slab thickness changes from 1 mm to 20 mm, the absorption peak shifts gradually to low frequency (from 30 GHz to 1 GHz). In other words, for the same absorption band, the frequency of absorption peak decreases with the increase of d. On the other hand, for higher excitation frequencies, with the increase of d, several higher-order modes appear, and the corresponding spectral bands are formed on the absorption spectrum. Hence, the frequencies of absorption peak can be easily tuned by changing the glass-slab thickness. Note that the lower-order resonances mode has a slightly broader bandwidth than that of higher-order one, as shown by the white dashed line in Fig. 2(b), which facilitates broadband operation and provides better experimental verification tolerance.

Figure 2(c) shows the effects of d on microwave absorption at interested frequency range. As a representative, we choose several different thicknesses that support the lowest order model for analysis. As shown in Fig. 2(c), the maximum absorption remains almost unchanged in magnitudes, and it shifts to lower frequencies with the increase of glass-slab thickness. Fig. 2(d) shows the corresponding results of R and T. R has the complementary variation to the absorption, and T remains almost unchanged, indicating that the shielding effect (SE) calculated by $SE\,(\text{dB}) = -10\log_{10}\text{T}$ is insensitive to the thickness d. When $d = 2$ mm, the microwave absorption is more than 90% in the frequency range from 12.1 GHz to 16.7 GHz with the maximum absorption 99.5% and minimum reflection -44.5 dB at 14.4 GHz, as well as good shielding efficiency (24 dB).

In order to further analyze the microwave performance of the proposed MA, we study the effects of sheet resistance and incidence angle on microwave absorption, reflection, and transmission. Fig. 3(a)

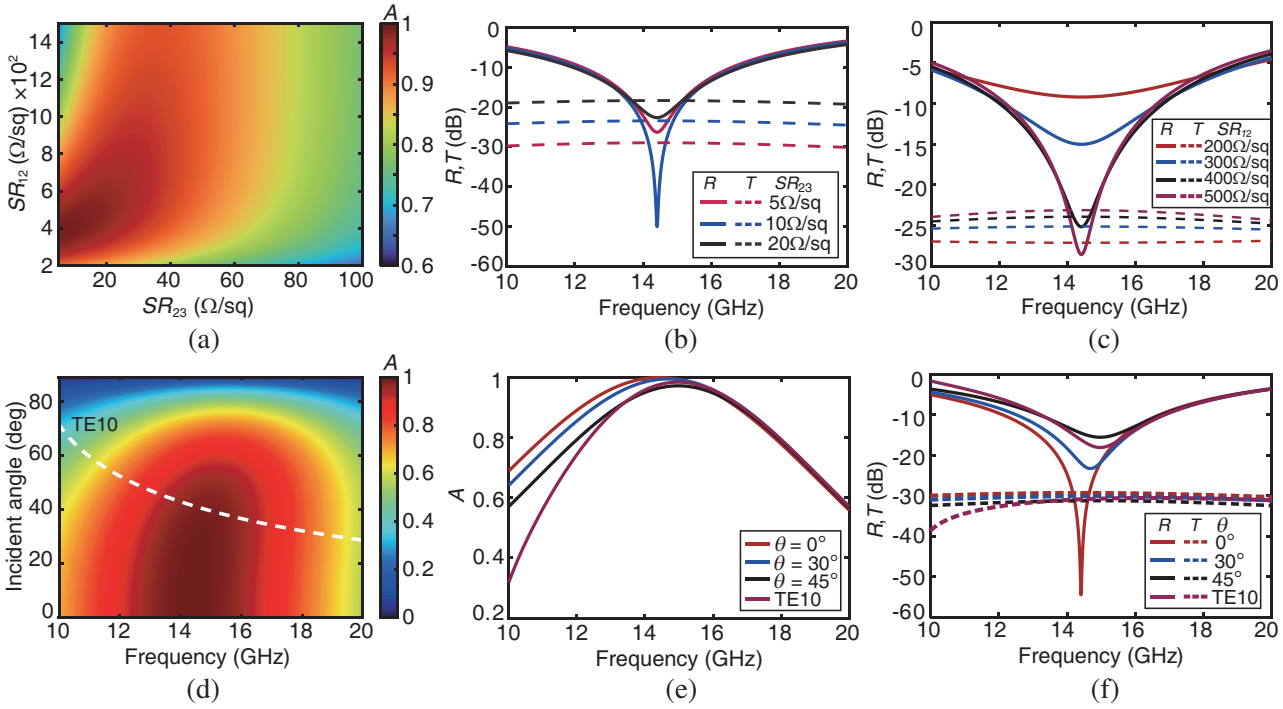

Figure 3. Effects of sheet resistance and incidence angle on the performance of MA for TE wave. (a) Calculated microwave absorption spectra as a function of sheet resistance at 15 GHz for normal incidence case. (b), (c) Effects of sheet resistance on R and T, (b) when $SR_{12} = 460\,\Omega$/sq, and (c) when $SR_{23} = 10\,\Omega$/sq for normal incidence case. (d) Calculated microwave absorption spectra as a function of incidence angle and excitation frequency. (e), (f) Effects of incidence angle on (e) A and (f) R and T, respectively. Here, the sheet resistance is $SR_{12} = 415\,\Omega$/sq and $SR_{23} = 5\,\Omega$/sq for (d)–(f), $d = 2.0$ mm for (a)–(f).

shows the calculated microwave absorption spectra by varying the sheet resistance of ITO films at the excitation frequency 15 GHz. As shown in Fig. 3(a), the MA shows good absorption performance when bottom ITO film (SR_{23}) has a small sheet resistance value, whereas the top ITO film (SR_{12}) has a large selectable resistance range, which allows us to easily carry out experimental verification. Figs. 3(b) and 3(c) show the effect of sheet resistance on R and T when $SR_{12} = 460\,\Omega$/sq and $SR_{23} = 10\,\Omega$/sq, respectively. As shown in Figs. 3(b) and 3(c), the ITO film with lower sheet resistance value provides better shielding effect when the bottom or top ITO film is fixed, since the lower sheet resistance provides higher reflection and therefore lower transmission. However, the high reflection is non-ideal for military applications such as perfect microwave absorption and stealth. Therefore, in the actual design, we need to weigh the reflection and transmission.

To study angle adaptability, we also characterized the performance for oblique incidence of TE waves (see supply materials S2 for more details about TM wave incidence case). Fig. 3(d) shows the calculated microwave absorption spectra as a function of incidence angle and excitation frequency. The MA exhibits broad absorption bandwidth and efficient absorption performance in a large range of incidence angle. The effect of incidence angle on A, R, T is shown in Figs. 3(e) and 3(f). With the increase of incidence angle, the value of peak absorption decreases due to larger reflection as shown in Fig. 3(f), and its absorption peak shifts to higher frequency as shown in Fig. 3(e), because a larger incidence angle produces a smaller k_z component, resulting in a smaller phase change. In order to compensate for the decrease of k_z component, the microwave frequency needs to be increased. When $SR_{12} = 415\,\Omega$/sq and $SR_{23} = 5\,\Omega$/sq, the cavity achieves good shielding efficiency (about 30 dB within 45° incidence angle), small reflection (−54.5 dB at 14.4 GHz), as well as the maximum absorption 99.9%, and the effective absorption band is from 12.1 GHz to 16.7 GHz and from 13.2 GHz to 16.8 GHz for 0° and 45° incidences, respectively. For comparison, we also give the microwave absorption, reflection

and transmission of TE10 mode as shown in Figs. 3(e) and 3(f). The cutoff frequency of waveguide mode is given in supply materials S3 (see supply materials S3 for more details), and the incidence angle corresponding to TE10 mode is shown in Fig. 3(d).

We have proposed a design method of transparent perfect MA and given the theoretical calculation and analysis. The microwave characteristics are related to the thickness of glass slab and sheet resistance of ITO films. The operating frequency and absorption peak can be adjusted according to the thickness of glass slab and the sheet resistance of films, which can also be replaced by graphene for which the sheet resistance of several hundred ohms is also relatively easy to achieve. For $SR_{23} = 10\,\Omega$/sq, the MA exhibits maximum absorption 99.5% at 14.4 GHz with a 4.6 GHz effective bandwidth, and the SE is 24 dB. On the other hand, better microwave reflecting layer (smaller SR_{23}) provides higher microwave shielding effect. For example, for $SR_{23} = 5\,\Omega$/sq, the MA exhibits maximum absorption 99.9% at 14.4 GHz with a 4.6 GHz effective bandwidth, and the SE is 30 dB. However, the processing difficulty may increase, and the optical performance will decline.

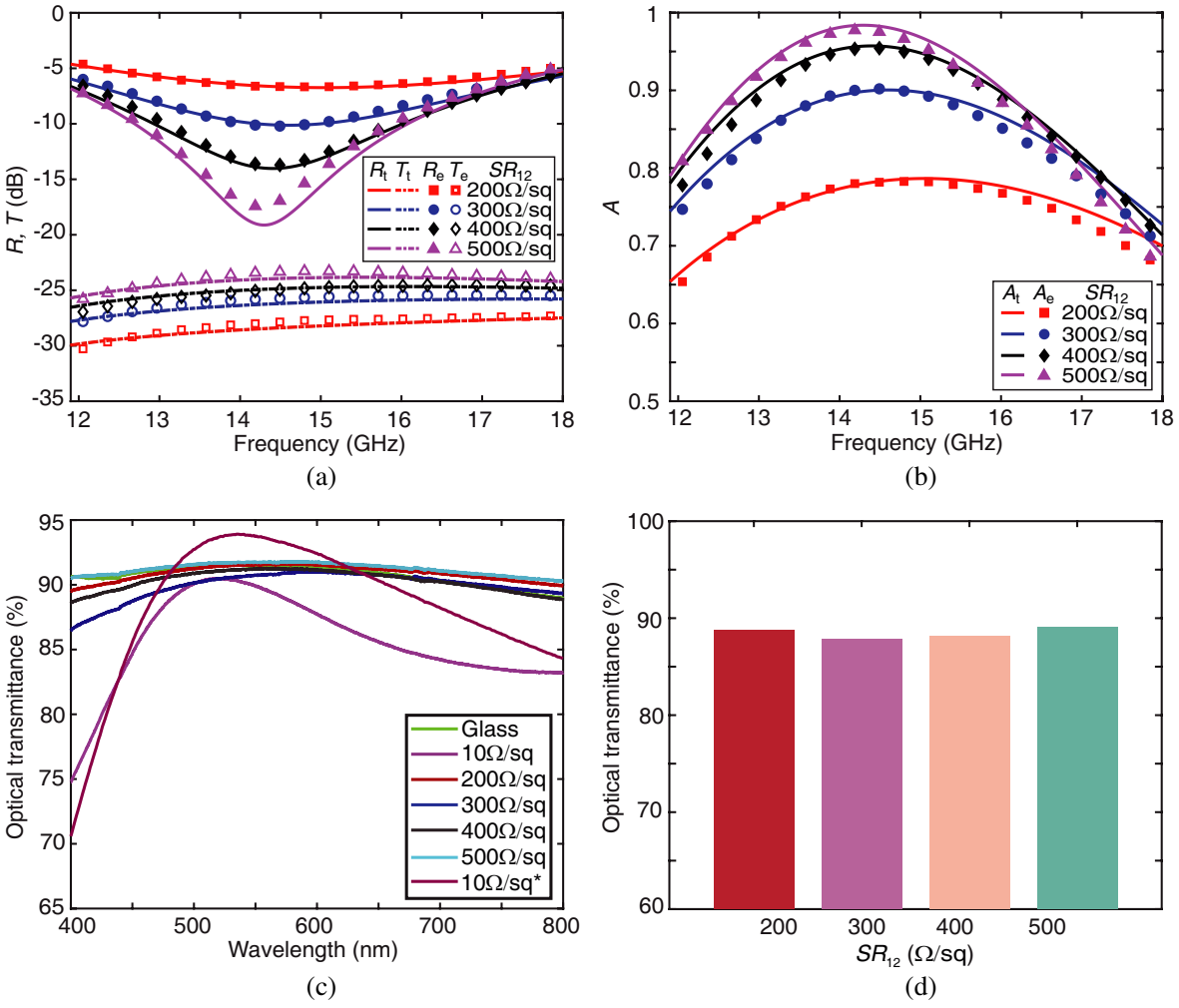

Figure 4. Comparison between measured and theoretical (a) reflection spectrum and transmission spectrum and (b) absorption spectrum for TE10 mode. The parameters are SR_{23}=10 Ω/sq and SR_{12}=200 Ω/sq, 300 Ω/sq, 400 Ω/sq, and 500 Ω/sq, respectively. (c), (d) Optical transmittance spectra of (c) glass without and with ITO film and (d) average transmittance in the spectral range from 400 nm to 800 nm of MAs with different sheet resistances as the top layer, where the SR_{23} is 10 Ω/sq*. The glass-slab thickness is $d = 2.2$ mm. Asterisk indicates ITO coated with antireflection coating.

2.3. Realization of Transparent Microwave Shielding

In order to further verify the actual working performance of the proposed MA, several IDI-structured cavities are fabricated by magnetron sputtering ITO films on glass, where the ITO films with minimized optical loss and suitable sheet resistance are necessary. We measure R and T of the fabricated devices from 11.9 GHz to 18 GHz with a waveguide. For comparison, microwave reflection, transmission, and absorption are theoretically calculated, and experimental results (R_e, T_e, A_e) are in good agreement with the theoretical results (R_t, T_t, A_t) as shown in Figs. 4(a) and 4(b). The experimental results show that the MA exhibits low reflection, transmission, and high absorption performance (97.7%) with an effective absorption band from 12.8 GHz to 15.8 GHz for TE10 mode incidence when $SR_{12} = 500\,\Omega$/sq.

Note that the proposed IDI-structured cavities are difficult to form an optical cavity due to its millimeter-order thickness, which is several orders of magnitude larger than the wavelength of visible light, resulting in incoherence situation. The optical transmittance of MAs will be mainly determined by the lower sheet resistance ITO film, because high conductivity (low sheet resistance) indicates high electron density and large optical loss. The transparency of such IDI-structured cavities can be further improved by increasing the optical transmittance of each layer. To study their optical performance, we measure optical transmittance spectra in the range from 400 nm to 800 nm of the individual ITO films on glass substrate and MA with different sheet resistances as shown in the Figs. 4(c) and 4(d). The optical transmission spectra of ITO films with higher sheet resistance on glass substrate is close to that of glass, indicating the high optical transparency of ITO films with an averaged transmittance more than 90% in the interested spectral range from 400 nm to 800 nm. For the ITO film with sheet resistance 10 Ω/sq, at shorter wavelengths, it acts as an optical absorber, and its absorption increases towards the

Table 1. Microwave and optical properties of different optically transparent broadband microwave absorbers.

Transparent broadband MAs		Regions of over −90% absorption (GHz)	*SE*	Optical transmittance
Bow-lie shaped metamaterial absorbers by metal [24]		5.8 GHz–12.2 GHz	-	62%–74% (400 nm–700 nm)
Multi-layer graphene/polyethylene terephthalate structures [26]		23.5 GHz–26.8 GHz	19.1 dB	80.5% @500 nm
Bistealth structure [29]		7.7 GHz–18 GHz	-	10%–30% (400 nm–800 nm)
Graphene dielectric ultrathin doped silver [13]		12 GHz–15.6 GHz	26 dB	55%–74% (400 nm–1000 nm)
Windmill-shaped metamaterial absorbers by ITO [30]		8.3 GHz–17.4 GHz	-	77% (380 nm–760 nm)
JGM absorber [31]		25.2 GHz–35.2 GHz	-	77% (400 nm–1100 nm)
This work	Experimental	12.8 GHz–15.8 GHz for TE10 mode	24.3 dB	89% (400 nm–800 nm) 94% @550 nm
	Theoretical	12.2 GHz–16.7 GHz for normal incidence	24 dB	

ultraviolet regime; however, its reflection increases towards the infrared regime. As a consequence, the ITO film with sheet resistance 10 Ω/sq exhibits an averaged optical transmission of only 85.7%. To improve its optical transmission, the antireflection coating is employed, which can realize an averaged optical transmission of 88.6%. The average transmittance of the proposed MA is 89.0% and insensitive to SR_{12} since the film at 1, 2 interface is as thin as tens of nanometers compared to the 180 nm ITO film at 2, 3 interface. Specifically, the transmittance is more than 94% near 550 nm (see Section S4 of the Supporting Information for details).

Table 1 shows the microwave absorption, shielding efficiency, and optical transmittance reported for different optically transparent MAs. The IDI-structured cavities prepared in this study could achieve a microwave *SE* of 24.3 dB with a 3 GHz effective bandwidth for TE10 mode experimentally and that of about 24 dB with a 4.5 GHz effective bandwidth for normal incidence theoretically as shown in Table 1. The average optical transmittance of the IDI-structured absorber is 89% from 400 nm to 800 nm, which is outstanding among the transparent MAs. In addition, the proposed IDI-structured microwave absorber does not require the complex nanofabrication process and can be fabricated easily.

3. CONCLUSIONS

In summary, we experimentally demonstrated a high transparent perfect MA based on an impedance-assisted Fabry-Pérot cavity consisting of transparent ITO films and glass slab. We explain the physical mechanism using multi-beam interference theory and calculate microwave reflection, transmission, and absorption theoretically for different glass-slab thicknesses, sheet resistances, and incidence angles. For verifying the actual working performance of the proposed MA, we fabricate several IDI-structured MAs by magnetron sputtering ITO films on glass and measure their microwave and optical properties. The experimental results are in good agreement with our theoretical results, which show a maximal absorption up to 97.7% at 14.3 GHz for TE10 mode incidence and a microwave *SE* of 24.3 dB with an averaged optical transmittance of near 90%. Furthermore, the theoretical results show that the MA can realize a maximal absorption up to 99.5% with a 4.5 GHz effective bandwidth for normal incidence. In addition, the proposed IDI-structured MA is easy to tune by simply altering the glass-slab thickness or the sheet resistance applying electrostatic gating when replacing the top ITO film with graphene. The proposed configuration and physical insight provide a new pathway for designing high performance microwave absorbers for effective transparent microwave shielding application and developing multifunctional microwave optical devices.

Methods:

Fabrication: The ITO films and optical antireflection coating are obtained using Denton Discovery-635 magnetron sputtering. Before the film deposition, the substrates were ultra-sonicated and cleaned in acetone, ethanol, and deionized water. The sputtering power is set at 300 W. ITO films with different resistances are prepared by controlling the sputtering time and thickness. The thickness of ITO film with low sheet resistance is around 180 nm, and those of ITO films with high sheet resistance are about 10 nm–20 nm.

Characterization: The thickness is measured by the spectroscopic ellipsometry (UVISEL, Hariba). The sheet resistances of ITO films are measured by a standard four-probe method [32] using a self-built microscope-based probe station. The optical transmittance is measured by a UV/Vis spectrophotometers (723PC, Shanghai Jinghua) ranging from 400 nm to 800 nm with normal incidence. The microwave reflection and transmission of MAs are measured using a Vector Network Analyzer (3672, Ceyear) by the standard waveguide measurement method ASTM D5568-14 [33].

ACKNOWLEDGMENT

The work was sponsored by the National Natural Science Foundation of China (NNSFC) under Grants No. 62005237, No. 62175217, No. 62071418, 61931007, U20A20164 and 61975177, the Science Challenge Project under Grant No. TZ2018002, and the Chaoyong Plan under Grant No. 130000-171207723/012.

REFERENCES

1. Ma, L., Z. Lu, J. Tan, J. Liu, X. Ding, N. Black, T. Li, J. Gallop, and L. Hao, "Transparent conducting graphene hybrid films to improve Electromagnetic Interference (EMI) shielding performance of graphene," *ACS Appl. Mater. Interfaces*, Vol. 9, 34221–34229, 2017.
2. Zhu, X., J. Xu, F. Qin, Z. Yan, A. Guo, and C. Kan, "Highly efficient and stable transparent electromagnetic interference shielding films based on silver nanowires," *Nanoscale*, Vol. 12, 14589–14597, 2020.
3. Yang, H., L. Wang, H. Wang, Y. Zhang, Z. Su, Z. Su, J. Zhang, Z. Lu, D. Jia, and P. Hu, "Transparent and high-absolute-effectiveness electromagnetic interference shielding film based on single-crystal graphene," *Adv. Mater. Technol.*, Vol. 7, 2101465, 2022.
4. Shu, J., W. Cao, and M. Cao, "Diverse metal-organic framework architectures for electromagnetic absorbers and shielding," *Adv. Funct. Mater.*, Vol. 31, 2100470, 2021.
5. Bakal, F., A. Yapici, M. Karaaslan, and O. Akgöl, "Microwave absorption performance of hexagonal nano boron nitride doped basalt fabric-reinforced epoxy composites," *Aircraft Engineering and Aerospace Technology*, Vol. 93, 205–211, 2021.
6. Li, Y., X. Tian, S. P. Gao, L. Jing, K. Li, H. Yang, F. Fu, J. Y. Lee, Y. X. Guo, and J. S. Ho, "Reversible crumpling of 2D titanium carbide (MXene) nanocoatings for stretchable electromagnetic shielding and wearable wireless communication," *Adv. Funct. Mater.*, Vol. 30, 1907451, 2020.
7. Chen, H., Y. Wen, Y. Qi, Q. Zhao, L. Qu, and C. Li, "Pristine titanium carbide MXene films with environmentally stable conductivity and superior mechanical strength," *Adv. Funct. Mater.*, Vol. 30, 1906996, 2020.
8. Lipatov, A., H. Lu, M. Alhabeb, B. Anasori, A. Gruverman, Y. Gogotsi, and A. Sinitskii, "Elastic properties of 2D Ti_3C_2Tx MXene monolayers and bilayers," *Sci. Adv.*, Vol. 4, eaat0491, 2018.
9. Shahzad, F., M. Alhabeb, C. B. Hatter, B. Anasori, S. M. Hong, C. M. Koo, and Y. Gogotsi, "Electromagnetic interference shielding with 2D transition metal carbides (MXenes)," *Science*, Vol. 353, 1137–1140, 2016.
10. Wen, B., M. Cao, M. Lu, W. Cao, H. Shi, J. Liu, X. Wang, H. Jin, X. Fang, and W. Wang, "Reduced graphene oxides: Light-weight and high-efficiency electromagnetic interference shielding at elevated temperatures," *Adv. Mater.*, Vol. 26, 3484–3489, 2014.
11. Grande, M., G. Bianco, M. Vincenti, D. De Ceglia, P. Capezzuto, V. Petruzzelli, M. Scalora, G. Bruno, and A. D'orazio, "Optically transparent microwave screens based on engineered graphene layers," *Opt. Express*, Vol. 24, 22788–22795, 2016.
12. Wang, H., Z. Lu, Y. Liu, J. Tan, L. Ma, and S. Lin, "Double-layer interlaced nested multi-ring array metallic mesh for high-performance transparent electromagnetic interference shielding," *Opt. Lett.*, Vol. 42, 1620–1623, 2017.
13. Wang, H., Y. Zhang, C. Ji, C. Zhang, D. Liu, Z. Zhang, Z. Lu, J. Tan, and L. J. Guo, "Transparent perfect microwave absorber employing asymmetric resonance cavity," *Adv. Sci.*, Vol. 6, 1901320, 2019.
14. Wang, W., B. Bai, Q. Zhou, K. Ni, and H. Lin, "Petal-shaped metallic mesh with high electromagnetic shielding efficiency and smoothed uniform diffraction," *Opt. Mater. Express*, Vol. 8, 3485–3493, 2018.
15. Jiang, Z.-Y., W. Huang, L.-S. Chen, and Y.-H. Liu, "Ultrathin, lightweight, and freestanding metallic mesh for transparent electromagnetic interference shielding," *Opt. Express*, Vol. 27, 24194–24206, 2019.
16. Han, Y., H. Zhong, N. Liu, Y. Liu, J. Lin, and P. Jin, "In situ surface oxidized copper mesh electrodes for high-performance transparent electrical heating and electromagnetic interference shielding," *Adv. Electron. Mater.*, Vol. 4, 1800156, 2018.
17. Ma, X., Y. Li, B. Shen, L. Zhang, Z. Chen, Y. Liu, W. Zhai, and W. Zheng, "Carbon composite networks with ultrathin skin layers of graphene film for exceptional electromagnetic interference shielding," *ACS Appl. Mater. Interfaces*, Vol. 10, 38255–38263, 2018.

18. Wang, C., V. Murugadoss, J. Kong, Z. He, X. Mai, Q. Shao, Y. Chen, L. Guo, C. Liu, and S. Angaiah, "Overview of carbon nanostructures and nanocomposites for electromagnetic wave shielding," *Carbon*, Vol. 140, 696–733, 2018.
19. Kim, Y., S.-K. Hyeong, Y. Choi, S.-K. Lee, J.-H. Lee, and H. K. Yu, "Transparent and flexible electromagnetic interference shielding film using ITO nanobranches by internal scattering," *ACS Appl. Mater. Interfaces*, Vol. 13, 61413, 2021.
20. Reshi, H. A., A. P. Singh, S. Pillai, R. S. Yadav, S. K. Dhawan, and V. Shelke, "Nanostructured $La_{0.7}Sr_{0.3}MnO_3$ compounds for effective electromagnetic interference shielding in the X-band frequency range," *J. Mater. Chem. C*, Vol. 3, 820–827, 2015.
21. Wang, A., W. Wang, C. Long, W. Li, J. Guan, H. Gu, and G. Xu, "Facile preparation, formation mechanism and microwave absorption properties of porous carbonyl iron flakes," *J. Mater. Chem. C*, Vol. 2, 3769–3776, 2014.
22. Kong, L. B., Z. Li, L. Liu, R. Huang, M. Abshinova, Z. Yang, C. Tang, P. Tan, C. Deng, and S. Matitsine, "Recent progress in some composite materials and structures for specific electromagnetic applications," *Int. Mater. Rev.*, Vol. 58, 203–259, 2013.
23. Hu, D., J. Cao, W. Li, C. Zhang, T. Wu, Q. Li, Z. Chen, Y. Wang, and J. Guan, "Optically transparent broadband microwave absorption metamaterial by standing-up closed-ring resonators," *Adv. Optical Mater.*, Vol. 5, 1700109, 2017.
24. Jang, T., H. Youn, Y. J. Shin, and L. J. Guo, "Transparent and flexible polarization-independent microwave broadband absorber," *ACS Photonics*, Vol. 1, 279–284, 2014.
25. Gupta, N. K., G. Singh, H. Wanare, S. A. Ramakrishna, K. V. Srivastava, and J. Ramkumar, "A low-profile consolidated metastructure for multispectral signature management," *J. Opt.*, Vol. 24, 035102, 2022.
26. Lu, Z., L. Ma, J. Tan, H. Wang, and X. Ding, "Transparent multi-layer graphene/polyethylene terephthalate structures with excellent microwave absorption and electromagnetic interference shielding performance," *Nanoscale*, Vol. 8, 16684–16693, 2016.
27. Wang, H., Y. Zhang, C. Ji, C. Zhang, Z. Lu, Y. Liu, Z. Cao, J. Yuan, J. Tan, and L. J. Guo, "High-performance transparent broadband microwave absorbers," *Adv. Mater. Interfaces*, Vol. 9, 2101714, 2022.
28. Shi, K., F. Bao, and S. He, "Enhanced near-field thermal radiation based on multilayer graphene-hBN heterostructures," *ACS Photonics*, Vol. 4, 971–978, 2017.
29. Zhang, C., X. Wu, C. Huang, J. Peng, C. Ji, J. Yang, Y. Huang, Y. Guo, and X. Luo, "Flexible and transparent microwave-infrared bistealth structure," *Adv. Mater. Technol.*, Vol. 4, 1900063, 2019.
30. Zhang, C., Q. Cheng, J. Yang, J. Zhao, and T. J. Cui, "Broadband metamaterial for optical transparency and microwave absorption," *Appl. Phys. Lett.*, Vol. 110, 143511, 2017.
31. Ma, L., H. Xu, Z. Lu, and J. Tan, "Optically transparent broadband microwave absorber by graphene and metallic rings," *ACS Appl. Mater. Interfaces*, Vol. 14, 17727–17738, 2022.
32. Kasap, S. O. and P. Capper, *Springer Handbook of Electronic and Photonic Materials*, 11, Springer, 2006.
33. Araz, İ. and F. Genç, "Development of broadband microwave absorber and measurement of its magnetic and microwave properties," *J. Supercond. Novel Magn.*, Vol. 31, 279–283, 2018.